European Radiology (2019) 29:770–782
https://doi.org/10.1007/s00330-018-5610-0

NEURO

The spectrum of brainstem malformations associated to mutations of the tubulin genes family: MRI and DTI analysis

Filippo Arrigoni[1] · Romina Romaniello[2] · Denis Peruzzo[1] · Andrea Poretti[3] · Maria Teresa Bassi[4] · Carlo Pierpaoli[5] · Enza Maria Valente[6,7] · Sara Nuovo[7,8] · Eugen Boltshauser[9] · Thierry André Gerard Marie Huisman[3] · Fabio Triulzi[10] · Renato Borgatti[2]

Received: 1 February 2018 / Revised: 15 May 2018 / Accepted: 15 June 2018 / Published online: 31 July 2018

Abstract

Objectives To describe the spectrum of brainstem malformations associated to mutations in the tubulin genes taking advantage of magnetic resonance imaging (MRI) and diffusion tensor imaging (DTI).

Methods Fifteen patients (six males; median age, 1.25 years; range, 1 month to 31 years) with mutations in the tubulin genes (*TUBA1A* = 8, *TUBB2B* = 4, *TUBB3* = 3) studied with MRI and DTI were included in the study. Brain MR exams were reviewed to describe the malformative aspects of the brainstem. Malformations of the supratentorial brain and cerebellum were also recorded. Tractography was performed in seven selected cases.

Results Fourteen patients (93%) showed complex malformations of the brainstem. Most common findings, apparent on anatomical MR sequences, were brainstem asymmetry (12 cases, 5 of which with a crossed pattern characterised by a hypertrophic right medulla oblongata and hypertrophic left pons), short and small pons on midline (10 cases) and anterior brainstem clefting (6 cases). DTI revealed abnormal transverse pontine fibres (13 cases), fusion of corticospinal tracts and medial lemnisci (9 cases) and a small decussation of the superior cerebellar peduncles (7 cases).

Conclusions Conventional/anatomical MRI and DTI reveal a complex pattern of brainstem malformations associated with tubulin genes mutations.

Key Points

- *Brainstem malformations affect 93% patients with mutated tubulin genes*
- *MRI shows homolateral and crossed brainstem asymmetries, clefts and pons hypoplasia*
- *DTI demonstrates irregular representation of transverse pontine fibres and fusion of corticospinal tracts*

Keywords Nervous system malformations · Brain stem · Tubulin · Diffusion tensor imaging · Neurological rehabilitation

Electronic supplementary material The online version of this article (https://doi.org/10.1007/s00330-018-5610-0) contains supplementary material, which is available to authorized users.

✉ Filippo Arrigoni
filippo.arrigoni@lanostrafamiglia.it

[1] Neuroimaging Lab, Scientific Institute, IRCCS E. Medea, Via Don Luigi Monza 20, 23842 Bosisio Parini, Lecco, Italy

[2] Neuropsychiatry and Neurorehabilitation Unit, Scientific Institute, IRCCS E. Medea, Bosisio Parini, Lecco, Italy

[3] Section of Pediatric Neuroradiology, Division of Pediatric Radiology, Russell H. Morgan Department of Radiology and Radiological Science, The Johns Hopkins University School of Medicine, Baltimore, MD, USA

[4] Laboratory of Molecular Biology, Scientific Institute, IRCCS E. Medea, Bosisio Parini, Lecco, Italy

[5] Quantitative Medical Imaging Section, National Institute of Biomedical Imaging and Bioengineering, National Institutes of Health, Bethesda, MD, USA

[6] Department of Molecular Medicine, University of Pavia, Pavia, Italy

[7] Neurogenetics Lab, IRCCS Santa Lucia Foundation, Rome, Italy

[8] Department of Medicine and Surgery, University of Salerno, Salerno, Italy

[9] Department of Paediatric Neurology, University Children's Hospital, Zurich, Switzerland

[10] Neuroradiology Department, Fondazione IRCCS Ca' Granda, Ospedale Maggiore Policlinico, Milano, Italy

Abbreviations

CST	Cortico-spinal tract
DEC	Directionally encoded colour
DMJD	Diencephalic-mesencephalic junction dysplasia
DTI	Diffusion tensor imaging
FA	Fractional anisotropy
HARDI	High angular resolution diffusion imaging
HGPPS	Horizontal gaze palsy and progressive scoliosis
MD	Mean diffusivity
PTCD	Pontine tegmental cap dysplasia
TPF	Transverse pontine fibres

Introduction

Tubulinopathies encompass a wide and emerging spectrum of brain malformations caused by mutations in the tubulin genes [1]. Tubulin genes encode different isotypes of proteins (α-, β- and γ-tubulin) that represent the major constituents of microtubules [2, 3] and are highly expressed during brain development, being involved in several fundamental processes like neuronal migration, cortical laminar organisation and neuronal guidance of the radial glia [4–7]. Mutations in tubulin genes (*TUBA1A, TUBA8, TUBB2A, TUBB2B, TUBB3, TUBB,TUBG1*) can alter the normal function and structure of microtubules, leading to complex congenital and non-progressive disorders of brain development characterised by severe brain malformations [2, 8, 9]. Only mutations in *TUBB4A* can result in a rare progressive form of leukodystrophy with hypomyelination, and atrophy of the basal ganglia and cerebellum [10, 11].

The neuroimaging features of tubulinopathies include commissural anomalies, basal ganglia and thalami dysmorphisms, malformations of cortical development (lissencephaly, pachygyria, schizencephaly, polymicrogyria and others), brainstem anomalies [8, 9, 12] and cerebellar cortical dysplasia [13, 14].

Supratentorial and cerebellar malformations have been extensively described with conventional/anatomical magnetic resonance imaging (MRI), but brainstem abnormalities have not been extensively investigated. The occurrence of brainstem hypoplasia or asymmetry has been reported with different frequencies (31-80%) [2, 8, 13]; however, without further morphological characterisation. Similarly, advanced MRI, in particular diffusion tensor imaging (DTI), has been used to elucidate the pattern of the supratentorial anomalies [5, 15, 16], but it has not yet been used to study the infratentorial anomalies in detail.

As demonstrated in many other brainstem malformations (e.g. Joubert syndrome, horizontal gaze palsy with progressive scoliosis, pontine tegmental cap dysplasia, diencephalic–mesencephalic junction dysplasia) [17–27], DTI may render valuable structural and architectural information about the normal and abnormal course and organisation of white matter tracts within the brainstem.

The aim of our study was to extend and fully characterise the spectrum of brainstem malformations by conventional/anatomical MRI and to investigate the morphology of white matter tracts within the brainstem by DTI in a cohort of children with confirmed tubulinopathies.

Materials and methods

Patients with a proven mutation in genes of the tubulin family were selected from the MRI database of E. Medea Research Institute and from the institutional collections of the other authors (T.H, E.V, E.B). The Ethics Committee of E. Medea Research Institute approved this study and written informed consent for MRI was obtained from all participating families.

The inclusion criteria were:

- Proven mutation on peripheral blood cells in a gene of the tubulin family
- Brain MR examination including morphological sequences (T1 and/or T2-weighted) in at least two orthogonal planes, including axial sections
- DTI sequence with at least 32 directions acquired with *b* values of at least 700 s/mm^2

The settings of MR sequences (both anatomical and DTI) were not homogeneous among the 15 patients that fulfilled the inclusion criteria. All patients except one were studied at 3 T. For the seven patients acquired at E. Medea Research Institute, the protocol included a three-dimensional T1-weighted MPRAGE sequence (voxel size, 1 × 1 × 1 mm^3), two T2-weighted turbo spin echo sequences in orthogonal planes (voxel size, 0.4 × 0.4 × 3 mm^3), one T2-weighted fast spin echo sequence (voxel size, 1.5 × 1.5 × 1.5 mm^3) and a two-shell DTI sequence with 4 *b*0 volumes, 8 directions at b = 300 s/mm^2, 32 directions at b = 1,100 s/mm^2 (voxel size, 2 × 2 × 2 mm^3).

The remaining eight subjects were acquired in four different centres. For all of them the acquisition protocol included a T1-weighted sequence (voxel size ranging from 0.35 × 0.35 × 3 mm^3 to 1 × 1 × 1 mm^3) and a DTI sequence with up to 4 *b*0 and 32-40 directions acquired at b = 700 s/ mm^2 or b = 1,000 s/mm^2 according to the patient age (in-plane resolution ranged from 0.7 × 0.7 to 2 × 2 mm^2 and the slice thickness ranged from 2 to 3 mm). T2-weighted sequences were also acquired with different parameters (in-plane resolution ranging from 0.4 × 0.4 mm^2 to 0.57 × 0.57 mm^2 and slice thickness ranging from 2.5 mm to 3.3 mm).

DTI data were processed with TORTOISE software [28] in order to obtain mean diffusivity (MD), fractional anisotropy (FA) [29] and directionally encoded colour (DEC) [30] maps. Raw data were corrected for motion and distortion artefacts (e.g. eddy current, B_0 susceptibility, echo-planar imaging distortion) using a structural image as reference [31]. Subsequently, data

were visually inspected for detection of remaining artefacts and to discard corrupted volumes. Finally, the DTI tensor was computed using a non-linear least square estimator [32] and the final parametric maps were derived.

Both conventional MR images and DTI maps were systematically reviewed by two authors (F.A and A.P) with more than 10 years of experience in paediatric neuroradiology each. Anatomical malformations seen on conventional MRI and structural alterations of white matter tracts on matching DTI maps were reported in consensus. In particular, asymmetries were assessed comparing the two sides of each brainstem section on multiple contiguous slices (T1 and/or T2-weighted images). No volumetric analysis of the brainstem was performed.

Tractography with TrackVis [33] was performed using the FACT algorithm (FA threshold was automatically selected by the software; angle threshold was 35°) in seven selected cases to better visualise the (re-)organisation of the white matter tracts in the brainstem.

Because of the wide distribution of patients' age, the small number of subjects and the heterogeneous DTI protocols, we did not perform statistical analysis of DTI derived parameters (FA, MD, etc.).

Genetic analysis of the mutated patients has been performed at E. Medea Research Institute by using a customised targeted resequencing NGS panel containing a specific set of genes (149) involved in malformations of cortical development and in other cerebral and cerebellar malformations (the list of genes is available upon request). The gene panel was designed using the Sure Design tool from Agilent (Agilent Technologies). NGS was performed using the MiSeq and NextSeq550 instruments (Illumina) using a SureSelect target enrichment system capture Process kit (Agilent Technologies). Variant calling and filtering have been performed with ANNOVAR [34] selecting for exonic and splice site variants with MAF >1%, leading to missense, nonsense or frameshift consequences. Damaging effects were predicted based on five prediction tools: Phastcons, PhyloP, SIFT, GERP and Polyphen. Human Splicing Finder v. 3.0 (HSF3.0) and ESEfinder v. 3.0 (ESE3.0) were used for in silico analysis. Variants detected were validated by Sanger sequencing. Mutation nomenclature is according to the recommendations of the Human Genome Variation Society and refers to the published *TUBA1A*, *TUBB2B* and *TUBB3* cDNA sequences (Acc. NM_006009.3, NM_178012.4 and NM_006086.3 respectively) with nucleotide +1 corresponding to the A of the ATG translation initiation codon.

Results

Population

Fifteen patients (male/female ratio, 6:9; mean age, 4.7 ± 8.2 years; median age, 1.25 years; range, 1 month to 31 years) with mutations in the tubulin genes were selected: eight subjects carried mutations in *TUBA1A* gene, four in *TUBB2B* gene and three in *TUBB3* gene. The genetic study on patients' parents showed that all variants occurred de novo. Main clinical data are summarised in Table 1. All patients showed developmental delay and motor impairment signs. Present or past history of epileptic seizures was documented in six cases, four of which had associated malformations of cortical development. Disturbances of ocular movements (strabismus and/or nystagmus) affected eight patients.

MRI findings

In 14/15 cases (93%) the brainstem showed malformative features on T1- and T2-weighted sequences (Fig. 1).

Twelve patients had a moderate to marked brainstem asymmetry that in two cases involved only the pons and in ten involved more than one segment including pons + medulla oblongata (hereafter "medulla") and/or mesencephalon. In five of twelve cases, the asymmetry was crossed between medulla and pons (i.e. hypertrophic right medulla and hypertrophic left pons). Five patients with asymmetry and one with no asymmetry had an anterior brainstem cleft. On midsagittal planes, the pons appeared short and small in ten cases. In one of ten, a small posterior pontine cap was observed (Fig. 2). The middle cerebellar peduncles appeared short in five children and asymmetric in two.

The ponto-mesencephalic junction was thin in four children and thick in one child, while the mesencephalon appeared thick in one child and clearly asymmetric in three other children. A thickened tectum was observed in two cases.

Vermis hypoplasia or rotation could be detected in ten cases and cerebellar dysplasia (i.e. folia malorientation) was present in nine cases (Table 2).

All patients had malformations of the supratentorial brain that involved the corpus callosum, anterior commissure, basal ganglia and thalami. Malformations of cortical development, including polymicrogyria and schizencephaly, were detected in eight children (Table ESM1).

DTI findings

The inspection of the FA and DEC maps revealed valuable information about the structure and organisation of the main white matter tracts within the malformed brainstems (Table 3).

The inferior cerebellar peduncles could easily be detected in eight patients while in seven children their integrity could not be assessed due to limited resolution. The middle cerebellar peduncles were short or asymmetric in seven children and had an abnormal orientation (purple/white colour on DEC maps) in eight cases. The superior cerebellar peduncles appeared normal in all children; however, their decussation

Table 1 Clinical and genetic data

Patient	Genetic findings	Gender	Age at MR (years)	Age at last follow-up (years)	Microcephaly	Developmental delay	Motor functions	Epilepsy	Ocular findings
1	TUBA1A	m	0.1	2.5	Yes	Moderate	Bilateral spasticity	Focal seizures	No
2	TUBA1A	m	0.6	3.5	Yes	Moderate	Bilateral spasticity	No	No
3	TUBA1A	f	0.8	3	Yes	Moderate	Diffuse hypotonia	West syndrome, generalised seizures	ONH, visual impairment, nystagmus
4	TUBA1A	f	0.8	1.6	Yes	Severe	Diffuse hypotonia, dystonia-dyskinesia	No	Strabismus, nystagmus
5	TUBA1A	m	1.0	3.5	No	Mild	Mild impairment	No	Strabismus
6	TUBA1A	f	1.3	1.6	Yes	Severe	Diffuse hypotonia	No	Strabismus, nystagmus
7	TUBA1A	f	5.0	8.5	Yes	Severe	Clumsiness, mild gait ataxia	No	Strabismus
8	TUBA1A	f	11.5	11.6	NA	Severe	Clumsiness, gait ataxia	West syndrome, focal complex seizures	Strabismus, nystagmus, left ptosis
9	TUBB2B	m	1.1	3.5	Yes	Moderate	Unilateral spasticity (left)	Focal seizures	Ptosis
10	TUBB2B	m	4.5	4.9	Yes	Moderate	Bilateral spasticity	Spasms	No
11	TUBB2B	f	8.3	12.9	Yes	Severe	Bilateral spasticity	Focal complex seizures	Strabismus, right ptosis
12	TUBB2B	f	31.8	30.7	Yes	Severe	Bilateral spasticity	West syndrome, focal complex seizures	ONH, OA, strabismus, nystagmus
13	TUBB3	f	1.1	1.1	No	Moderate	Facial diplegia	No	Bilateral ptosis, strabismus, nistagmus paralysis of the 3rd, 4th, 7th Bilaterally
14	TUBB3	m	1.3	1.2	No	Moderate	Diffuse hypotonia	No	Strabismus, nystagmus, OA
15	TUBB3	f	2.0	4.5	Yes	Moderate	Diffuse hypotonia, dystonia	No	No

f female, *m* male, *NA* not available, *OA* optic atrophy, *ONH* optic nerve hypoplasia

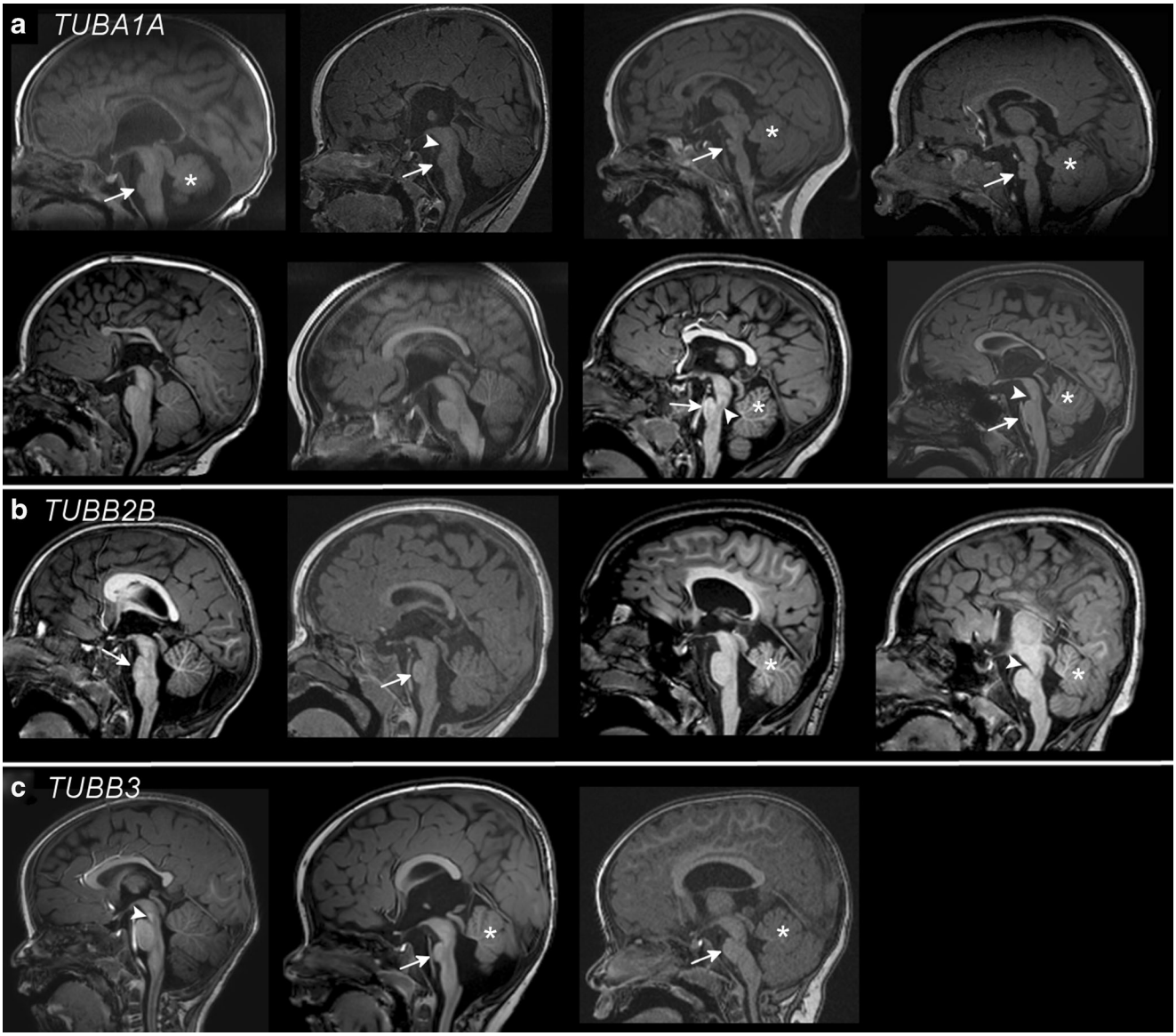

Fig. 1 Brainstem appearance on sagittal sections. Midline T1-weighted sections show the heterogeneity of midbrain-hindbrain dysmorphisms in patients with mutations in *TUBA1A* (**a**), *TUBB2B* (**b**) and *TUBB3* (**c**) genes. Pons hypoplasia (*arrows*), irregular ponto-mesencephalic junction (*arrowheads*) and vermis hypoplasia (stars) could be noted in several patients. Corpus callosum malformation are also evident in all patients

(usually visible as a red spot on DEC maps in the mesencephalon) appeared reduced in seven cases. The transverse pontine fibres (TPF) had an abnormal presentation in 13 of 15 subjects. The dorsal component of TPF was markedly reduced or absent in 12, while the anterior component was reduced in only one child. A thickened anterior component was detected in five children (Fig. 3).

The corticospinal tracts (CSTs) and the medial lemnisci appeared to be fused on axial DEC maps at the pontine level in nine children and reduced or asymmetric in four children. Asymmetry or hypoplasia and abnormal signal intensity of the CSTs at the level cerebral peduncles was evident in ten children (Fig. 3).

Tractography performed on the CSTs and TPF showed several combinations of tract asymmetries, thinning and thickening, confirming the abnormalities detected on the DEC maps (Fig. 4).

Discussion

Conventional/anatomical MRI and advanced/architectural DTI demonstrated a complex pattern of brainstem malformations in patients with mutations in *TUBA1A, TUBB2B* and *TUBB3* genes. The malformed shape of the brainstem corresponded to an altered organisation and

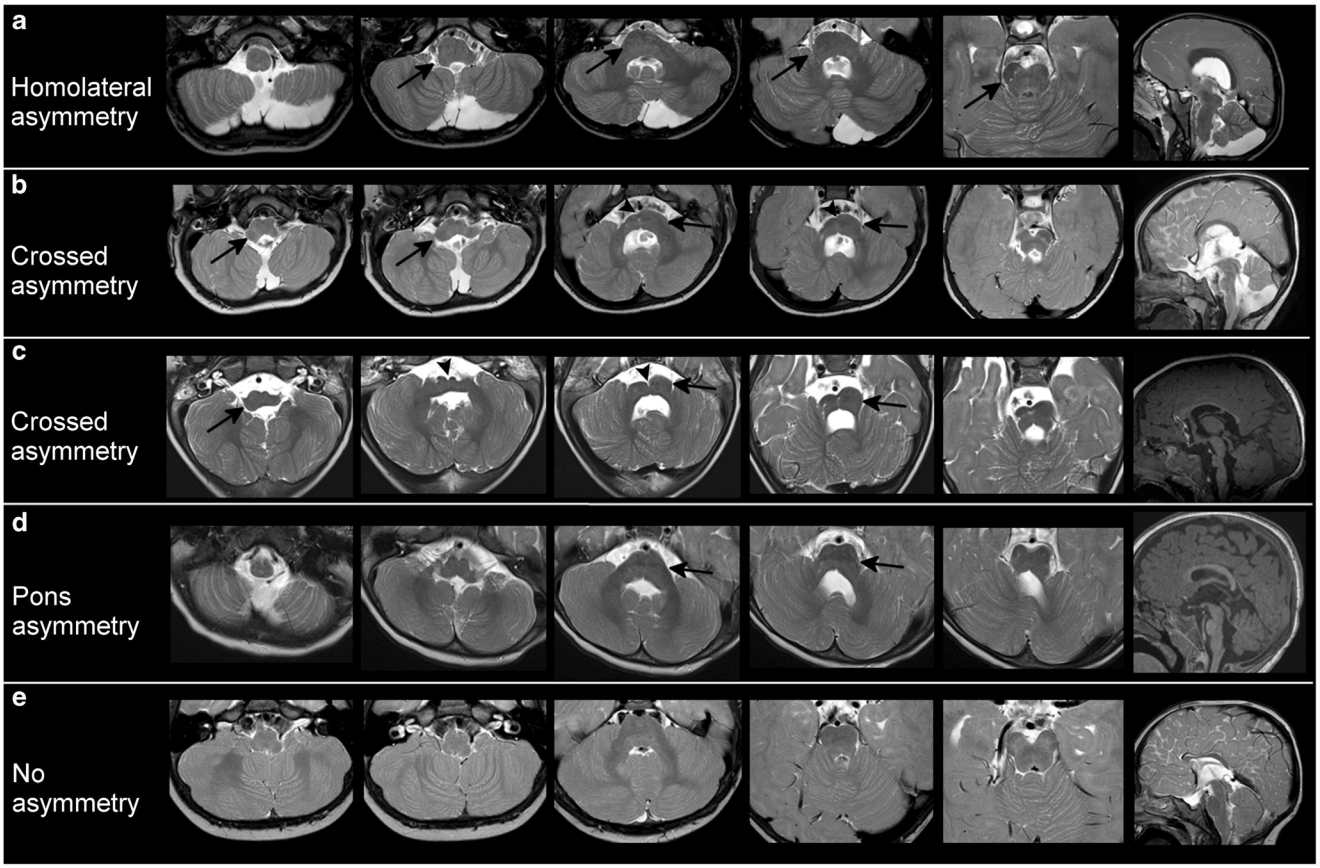

Fig. 2 Patterns of brainstem asymmetry. Axial T2-weighted sections of the brainstem, from the medulla to the mesencephalon, of five patients with different patterns of brainstem asymmetry are shown in *each row*. Sagittal T1 and T2-weighted sections are shown in the *last column of each row*. Patient A has an ipsilateral asymmetry with an enlargement of the right portion of medulla, pons and right cerebral peduncle (*arrows* in **a**). Patients B and C carry mutations on different genes (*TUBB3* and *TUBA1A* respectively) but share the same pattern of crossed brainstem asymmetry (right medulla > left medulla; right pons < left pons) (*arrows* in **b** and **c**) and an anterior midline cleft (*arrowheads* in **b** and **c**). Patient D shows an isolated pontine asymmetry (*arrow* in **d**), while patient E has no asymmetry

representation of brainstem white matter tracts (mainly CSTs and TPF) as shown by DTI.

The most frequent finding was an asymmetry (between the right and left side) of one or more segments of the brainstem (medulla, pons and mesencephalon), with either a consistently homolateral or crossed pattern. With "crossed pattern" abnormality we intend an abnormality that presents on one side at certain anatomical levels of the brainstem and then appears on the contralateral side at a different level (e.g. enlarged right medulla and left pons, or vice versa). With "homolateral pattern" we defined those cases where the hypertrophic (or hypotrophic) side of the brainstem is the same at different levels (e.g. enlarged right medulla and pons).

Cerebral asymmetries have been described in cerebral hemispheres—like in hemimegalenchephaly/dysplastic megalencephaly [35, 36]—or in the cerebellum as result of altered neuronal proliferation [due to mutations affecting the mammalian target of rapamycin (mTOR) pathway] [35]. Similar asymmetries have never been reported in the brainstem except for recent descriptions of tubulin-related malformations [12].

In our cohort, asymmetries between the two sides of the brainstem appeared related to asymmetries in the thickness of major white matter tracts (Table 3) more than to the presence of abnormal, ectopic tissue since no focal signal alterations were detected on T1- and T2-weighted images and MD maps. Histology or ultra-high resolution DTI may help to better characterise this finding.

In this series, brainstem clefts were quite frequent (40%), usually involving one or two segments of the brainstem (medulla and pons) while sparing the mesencephalon. The presence of an anterior cleft in the brainstem is a rare condition, documented in few syndromes like horizontal gaze palsy and progressive scoliosis (HGPPS) [20, 37] or diencephalic-mesencephalic junction dysplasia (DMJD) [21, 38, 39]. Intriguingly, HGPPS is due to mutations in *ROBO3*, a gene involved in mechanisms of axonal guidance similar to the tubulin genes [40, 41]. Even if the genetic mechanisms responsible for DMJD have not been identified, previous data

Table 2 Infra-tentorial MRI findings

Patient	Brainstem symmetry	Brainstem cleft	Pons appearance on midsagittal planes	MCP	P-M junction	Mesencephalon	Cranial nerves	IV ventricle	Vermis	Cerebellar cortex
1	Asymmetric pons (l > r)	No	Short and small	Regular	Regular	Regular. Thick tectum		Regular	Hypoplastic	Regular
2	No asymmetry	No	Regular	Regular	Regular	Regular		Regular	Regular	Regular
3	Asymmetric brainstem (r < l)	Anterior cleft in the medulla	Short and small	Short	Thick	Regular. Thick tectum		Dilated	Moderate vermis rotation	Malorientation of cerebellar folia (superior r hemisphere)
4	Asymmetric brainstem (r > l in the medulla; l > r in the pons)	Anterior cleft in the medulla and pons	Short and small	Short	Regular	Asymmetric		Dilated	Hypoplastic and rotated	Cerebellar cortical dysplasia
5	Mild asymmetric brainstem (r > l)	No	Regular	Regular	Regular	Regular		Regular	Regular	Regular
6	Asymmetric brainstem (r > l in the medulla; l > r in the pons)	Anterior cleft in the medulla and pons	Short and small	Short	Regular	Asymmetric		Mildly dilated	Hypoplastic and rotated	Cerebellar cortical dysplasia
7	No asymmetry	Small pontine cleft	Short and small	Short	Narrow	Regular		Mildly dilated	Hypoplastic and rotated	Maloriented hemispheres. No dysplasia
8	Asymmetric brainstem (r > l)	No	Short and small	Short	Narrow	Asymmetric		Regular	Hypoplastic	Malorientation of folia (r and l hemisphere)
9	Asymmetric pons (l >r)	No	Short and small	Thick left MCP	Regular	Regular		Mildly dilated	Regular	Malorientation of folia (superior r hemisphere)
10	Asymmetric brainstem (r > l)	No	Short and thinpons. Posterior right "cap"	Regular	Regular	Regular		Dilated	Regular	Maloriented hemispheres. No dysplasia
11	Mild asymmetric brainstem (r > l in the medulla; l > r in the pons)	No	Regular	Regular	Narrow	Thick	Thin right III nerve	Regular	Hypoplastic	Malorientation of folia (superior hemispheres r > l)
12	Mild asymmetric brainstem (r > l)	No	Regular	Regular	Regular	Regular		Mildly dilated	Hypoplastic and rotated	Malorientation of folia (superior r hemisphere)

Table 2 (continued)

Patient	Brainstem symmetry	Brainstem cleft	Pons appearance on midsagittal planes	MCP	P-M junction	Mesencephalon	Cranial nerves	IV ventricle	Vermis	Cerebellar cortex
13	No asymmetry	No	Regular	Regular	Narrow	Regular	Agenesis of III pair of nerves. Agenesis of left VII nerve; thinning of right VII nerve. Agenesis of olfactory bulbs	Regular	Regular	Regular
14	Asymmetric brainstem (r > l in the medulla; l > r in the pons)	Anterior cleft (pons > medulla)	Short and small	Thick left MCP	Regular	Regular		Dilated	Hypoplastic and rotated	Malorientation of folia (r hemisphere)
15	Mild asymmetric brainstem (r > l in the medulla; l >r in the pons)	Small pontine cleft	Short and small	Regular	Regular	Regular		Regular	Mildly Hypoplastic	Malorientation of folia (medial r hemisphere)

MCP middle cerebellar peduncles, *P-M Junction* ponto-mesencephalic junction

suggest the involvement of genes responsible of axonal guidance mechanisms [21, 22].

We also observed pons hypoplasia, frequently associated with vermian hypoplasia and cortical cerebellar dysplasia (i.e. malorientation of cerebellar folia) [14], suggesting that the whole hindbrain may be affected in tubulinopathies from a structural point of view. This is also supported by the altered orientation of MCP and the reduction of SCP decussation shown on the DEC maps.

The most relevant finding revealed by DTI analysis was the abnormal representation of, and irregular relationship between, CSTs and TPF. Such alterations may be the results of: (1) thinning/atrophy of CST; (2) abnormal course of CST; (3) thinning/thickening of TPF; (4) irregular course of TPF; (5) a combination of the previous factors. Anomalies in the course of CST were described or hypothesised in some malformative conditions like Joubert syndrome, HGPPS, Mobius syndrome and other disorders [19, 42–45]. Pyramidal tract malformations have been associated with defects in dorsal induction, cell proliferations, neuronal migration and guidance mechanisms [45].

Anomalies in the orientation and organisation of TPF have initially been reported in the Dandy-Walker syndrome [17], where transverse fibres are vertically elongated and caudally displaced and in pontine tegmental cap dysplasia (PTCD), where an abnormal transverse white matter bundle is present on the dorsal surface of the pons. Rollins et al. [27] recently widened the spectrum of TPF anomalies revealed by DTI in patients with brain malformations. The most frequent patterns among 31 children with brainstem anomalies were agenesis and hypoplasia of the dorsal component of TPF followed by CST irregular representation. The authors did not perform genetic testing for tubulin or other genes mutations; therefore, no genotype-phenotype correlation was possible. They hypothesised that pontine anomalies may be the results of derailed migration of precerebellar neurons, abnormal synaptogenesis or ineffective chemotactic signalling of pontine neurons. CST anomalies are supposed to be related to disruption of mechanisms involved in the regulation of axonal growth.

Brainstem abnormalities in tubulinopathies have been reported previously by different authors [2, 8, 12, 13]. Brainstem hypoplasia (in particular flattened pons) was the most reported finding, while asymmetries were described with a frequency of 37 to 100 % [12, 13]. In line with the literature, our cohort showed a flattened and short pons in 67% of patients and asymmetries in 80%. A pontine cleft/indentation was described in 80% of patients by Oegema et al. [13], while in our cohort brainstem clefts were detected in 40% of patients. A large tectum was described in 6/18 patients by Mutch et al. [12], while we found it only in two cases.

The other features we reported (e.g. crossed pattern of asymmetries, abnormal size of MCP or DTI abnormalities)

Table 3 DTI findings at the level of the brainstem

Patient	ICP	MCP	SCP	SCP decussation	Pontine transverse fibres	Medial lemnisci	CSTs-pons	CSTs-mesencephalon
1	n.a.	Regular	Regular	Regular	Reduced (the dorsal component is not clear)	Fused with CSTs	Fused with lemnisci	Small
2	Regular	Regular	Regular	Small	Regular	Regular	Regular	Regular
3	n.a.	Short, abnormal signal (red/white)	Regular	Small	Reduced (the dorsal component is not clear) + asymmetric	Fused with CSTs	Fused with lemnisci	Asymmetric
4	n.a.	Short, abnormal signal (white)	Regular	Small	Reduced (the dorsal component is not clear) + asymmetric	Fused with CSTs	Fused with lemnisci	Asymmetric
5	Regular	Abnormal signal (mild)	Regular	Regular	Regular	Regular	Mild asymmetry (l < r)	Regular
6	n.a.	Short, abnormal signal (white)	Regular	Small	Reduced (the dorsal component is not clear) + asymmetric	Fused with CSTs	Fused with lemnisci	Asymmetric
7	Regular	Short, abnormal signal (white)	Regular	Regular	Thick anterior component ; dorsal component not clear	Regular	Reduced	Small
8	n.a.	Short, abnormal signal (red/white)	Regular	Regular	Thick anterior component ; dorsal component not clear	Fused with CSTs	Fused with lemnisci	Asymmetric
9	Regular	Asymmetric (l > r)	Regular	Small	Thick anterior component; dorsal component not clear	Fused with CSTs	Reduced	Regular
10	Regular	Abnormal signal (red/white)	Regular	Regular	Reduced (the dorsal component is not clear)	Reduced	Reduced and asymmetric (l < r)	Asymmetric (l<<r)
11	Regular	Regular	Regular	Regular	Thick anterior component; dorsal component not clear	Regular	Regular	Bilateral abnormal signal
12	Regular	Regular	Regular	Regular	Reduced anterior component	Regular	Regular	Regular
13	Regular	Regular	Regular	Small	Thick anterior component; dorsal component not clear	Fused with CSTs	Fused with lemnisci	Regular
14	n.a.	Asymmetric (l > r). Right MCP looks white	Regular	Small	Reduced (the dorsal component is not clear) + asymmetric	Fused with CSTs	Fused with lemnisci	Small; pale colour
15	n.a.	Regular	Regular	Regular	Reduced (the dorsal component is not clear)	Fused with CSTs	Fused with lemnisci	Small; pale colour

ICP inferior cerebellar peduncles, *MCP* middle cerebellar peduncles, *SCP* superior cerebellar peduncles, *CST* corticospinal tract

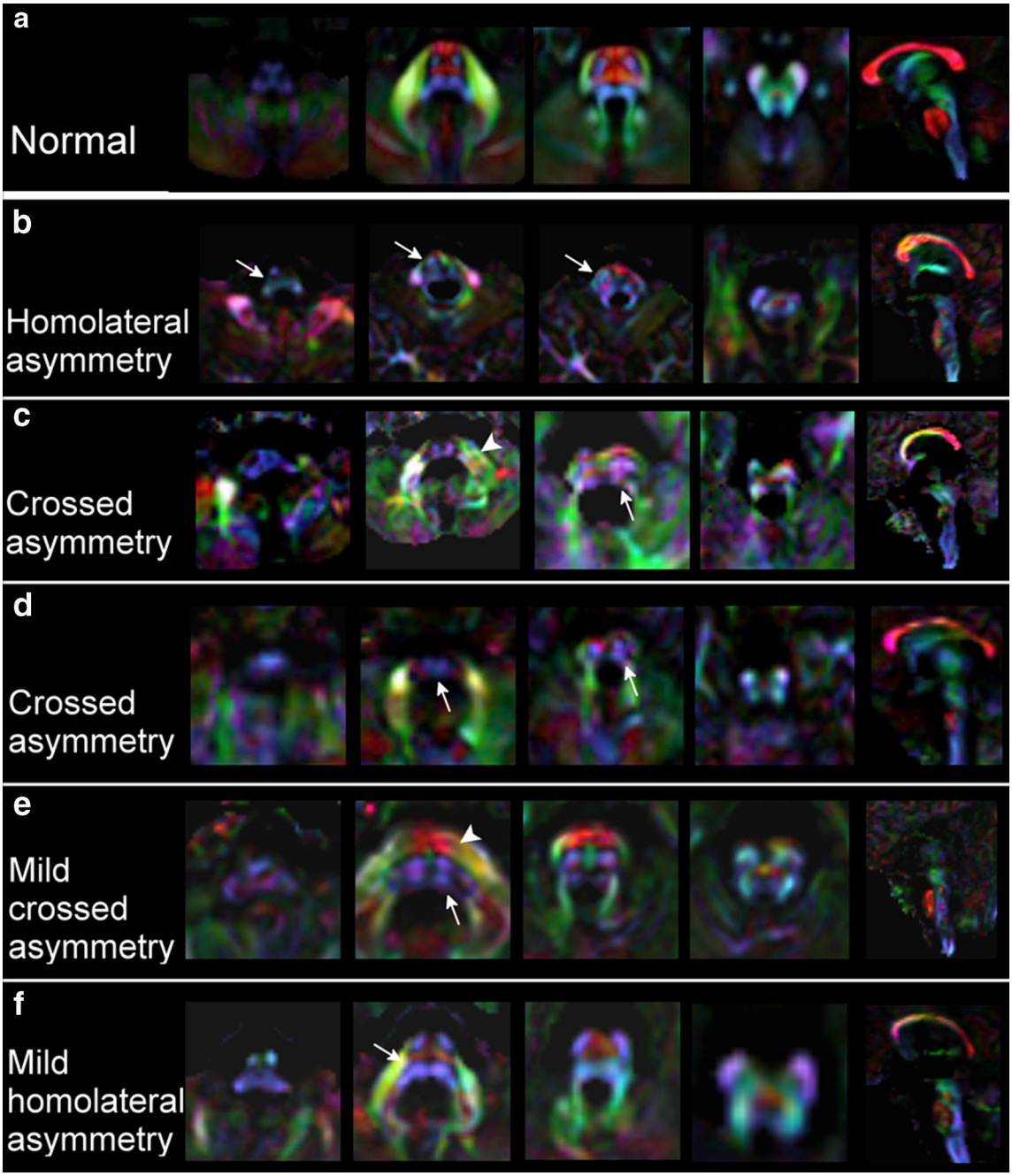

Fig. 3 DEC maps of the malformed brainstems. The DEC maps of five patients (**b**-**e**) with different patterns of brainstem malformation are compared to the maps obtained from the DTI template of typically developing 4-year-old subjects from the NIH study of normal brain development (**a**) [46, 47]. Lemnisci and CSTs can be enlarged/fused (*arrows* in **b**, **c** and **d**) or partially fused (*arrows* in **b**). Patients B, C and D show a thinning of anterior TPF and a complete deletion of posterior TPF. In patient E, only an anterior thick component of TPF is present, whereas in patient F, the anterior component is nearly absent while the posterior is preserved (*arrows* in **f**). Asymmetry of middle cerebellar peduncles can be found (*arrowhead* in **c**)

were not previously described and represent novel findings. Given the small number of patients per mutated gene, we did not perform a statistical genotype-phenotype correlation. However, when we looked at the frequencies of malformations in the three genes (Table 4), we noticed some interesting elements that need further confirmation on larger samples. In all mutated genes brainstem abnormalities were detected. In *TUBB2B* patients we did not find clefts and the frequency of SCP decussation thinning and fusion of CST with lemnisci was relatively low. The pattern of malformations was more similar between *TUBA1A* and *TUBB3* patients, except for abnormal MCP size that was particularly present in patients carrying mutations in *TUBA1A* gene.

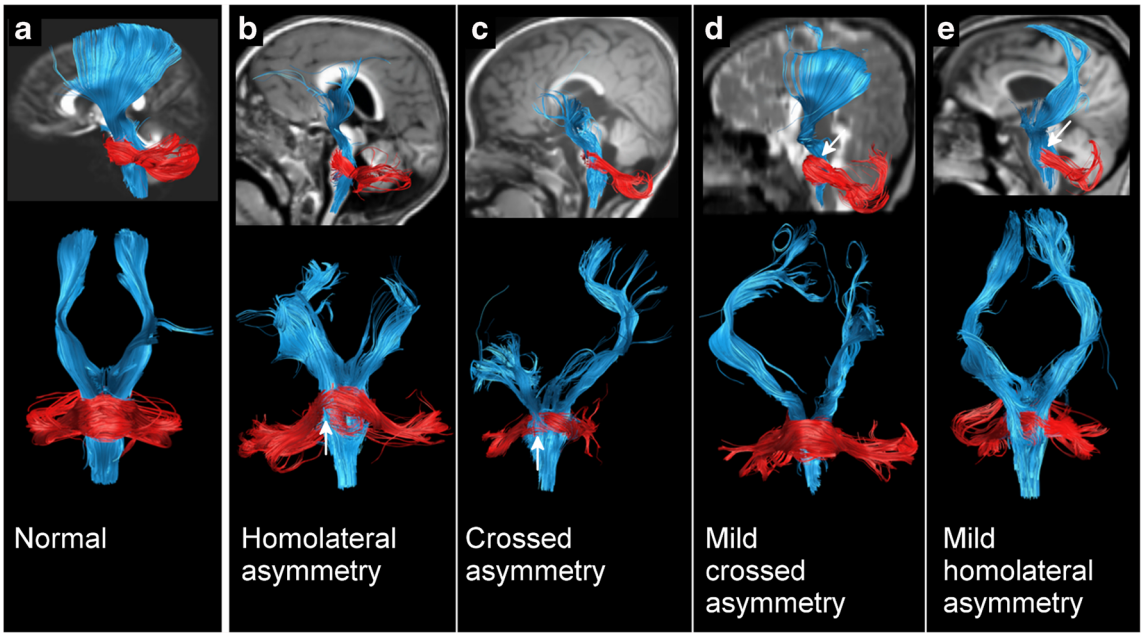

Fig. 4 Tractography of CST and TPF. Brainstem tractography of four malformed patients (**b**-**e**) is compared to normal tracts reconstructed from a template of normal subjects (**a**). Patients B and C (**b** and **c** in Fig. 3 as well) show a thinning of anterior TPF on the enlarged side of the pons, with CSTs that are close to the anterior bound of the brainstem. Patient D (**e** in Fig. 3) has a thick anterior TPF component, while the posterior one is not properly reconstructed by the algorithm (*arrow* in **d**). Patient E (**f** in Fig. 3) shows only the posterior component of TPF. CST are unilaterally thinned in **c** and **d**, while middle cerebellar peduncles are thinned in all cases

Given the established role of tubulin genes in axonal guidance [4], we hypothesise that the altered representation of white matter tracts in our patients may be caused by an impairment of these mechanisms during embryogenesis and brain development. The constant presence of disorganised white matter tracts suggests that disruption of axon growth and guidance, in addition to defects in neuronal migration, represents the peculiar features of tubulin-related disorders and lead us to define tubulin related conditions as a primary axonal guidance disorder [2].

Among the limitations of this study, we did not provide quantitative measures of brainstem asymmetries because of the lack of reference standard measures for brainstem segments during childhood. However, asymmetries were carefully identified by experienced paediatric neuroradiologists using different image weightings and planes. To be confirmed, the asymmetry should be present on three or more contiguous slices on the axial planes.

Given the retrospective nature of this study, we only had heterogeneous DTI protocols with maximum *b* values of 1,100 s/mm^2 and no more than 32 directions. The limitations of DTI in resolving crossing fibres and the resolution used in these acquisitions did not allow us to go into further details in the characterisation of brainstem tracts. Different approaches, like HARDI techniques, may contribute to unravel the complexity of white matter reorganisation in these patients.

In conclusion, our study expands the spectrum of malformations associated with tubulin genes mutations, revealing complex patterns of morphological and intrinsic white matter tracts anomalies at the level of the brainstem.

Table 4 Frequency of most relevant malformations per mutated gene

Finding	*TUBA1A* (8)	*TUBB2B* (4)	*TUBB3* (3)	All patients (15)
Brainstem asymmetry	75% (6)	100% (4)	67% (2)	80% (12)
Brainstem cleft	50% (4)	0% (0)	67% (2)	40% (6)
Pons hypoplasia on sagittal section	75% (6)	50% (2)	67% (2)	67% (10)
Abnormal size of MCP	63% (5)	25% (1)	33% (1)	47% (7)
Small SCP decussation	50% (4)	25% (1)	67% (2)	47% (7)
Abnormal PTF	75% (6)	100% (4)	100% (3)	87% (13)
Fused CST/lemnisci	63% (5)	25% (1)	100% (3)	60% (9)

The number of affected patients is reported in brackets

Acknowledgements This paper is dedicated to the memory of our dear friend and colleague, Andrea Poretti, an incredibly gifted and talented clinician, scientist and teacher who worked with us on the manuscript before his untimely demise. He will be in our memories forever.

We would like to thank Amritha Nayak for help in preparing Fig. 3.

Funding This study has received funding by the European Research Council (ERC Starting Grant 260888), the Pierfranco and Luisa Mariani Foundation (PADAPORT project) and the Italian Ministry of Health (Ricerca Corrente 2015-2016, Ricerca Finalizzata 2013 NET-2013-02356160, 5X MILLE fundings).

Compliance with ethical standards:

Guarantor The scientific guarantor of this publication is Dr. Filippo Arrigoni.

Conflict of interest The authors of this manuscript declare no relationships with any companies, whose products or services may be related to the subject matter of the article.

Statistics and biometry No complex statistical methods were necessary for this paper.

Informed consent Written informed consent was obtained from all subjects (patients) in this study.

Ethical approval Institutional Review Board approval was obtained.

Study subjects or cohorts overlap Some study subjects or cohorts have been previously reported in Romaniello R et al. (2017) Tubulin-related cerebellar dysplasia: definition of a distinct pattern of cerebellar malformation. Eur Radiol 27:5080-5092.

Methodology
- retrospective
- cross-sectional
- multicentre study

References

1. Bahi-Buisson N, Cavallin M (2016) Tubulinopathies Overview. In: Adam MP, Ardinger HH, Pagon RA, Wallace SE, Bean LJH, Stephens K, Amemiya A (eds) GeneReviews. University of Washington, Seattle
2. Romaniello R, Arrigoni F, Cavallini A et al (2014) Brain malformations and mutations in α- and β-tubulin genes: A review of the literature and description of two new cases. Dev Med Child Neurol 56:354–360. https://doi.org/10.1111/dmcn.12370
3. Chakraborti S, Natarajan K, Curiel J et al (2016) The emerging role of the tubulin code: From the tubulin molecule to neuronal function and disease. Cytoskeleton (Hoboken) 73:521–550. https://doi.org/10.1002/cm.21290
4. Tischfield MA, Baris HN, Wu C et al (2010) Human TUBB3 mutations perturb microtubule dynamics, kinesin interactions, and axon guidance. Cell 140:74–87. https://doi.org/10.1016/j.cell.2009.12.011
5. Poirier K, Saillour Y, Bahi-buisson N et al (2010) Mutations in the neuronal b-tubulin subunit TUBB3 result in malformation of cortical development and neuronal migration defects. Hum Mol Genet 19:4462–4473. https://doi.org/10.1093/hmg/ddq377
6. Jaglin XH, Chelly J (2009) Tubulin-related cortical dysgeneses: microtubule dysfunction underlying neuronal migration defects. Trends Genet 25:555–566. https://doi.org/10.1016/j.tig.2009.10.003
7. Tischfield MA, Cederquist GY, Gupta MLJ, Engle EC (2011) Phenotypic spectrum of the tubulin-related disorders and functional implications of disease-causing mutations. Curr Opin Genet Dev 21:286–294. https://doi.org/10.1016/j.gde.2011.01.003
8. Bahi-Buisson N, Poirier K, Fourniol F et al (2014) The wide spectrum of tubulinopathies: What are the key features for the diagnosis? Brain 137:1676–1700. https://doi.org/10.1093/brain/awu082
9. Romaniello R, Arrigoni F, Bassi MT, Borgatti R (2015) Mutations in α- and β-tubulin encoding genes: Implications in brain malformations. Brain Dev 37:273–280. https://doi.org/10.1016/j.braindev.2014.06.002
10. Simons C, Wolf NI, McNeil N et al (2013) A de novo mutation in the β-tubulin gene TUBB4A results in the leukoencephalopathy hypomyelination with atrophy of the basal ganglia and cerebellum. Am J Hum Genet 92:767–773. https://doi.org/10.1016/j.ajhg.2013.03.018
11. Tonduti D, Aiello C, Renaldo F et al (2016) TUBB4A-related hypomyelinating leukodystrophy: New insights from a series of 12 patients. Eur J Paediatr Neurol 20:323–330. https://doi.org/10.1016/j.ejpn.2015.11.006
12. Mutch CA, Poduri A, Sahin M et al (2016) Disorders of microtubule function in neurons: imaging correlates. AJNR Am J Neuroradiol 37:528–535. https://doi.org/10.3174/ajnr.A4552
13. Oegema R, Cushion TD, Phelps IG et al (2015) Recognizable cerebellar dysplasia associated with mutations in multiple tubulin genes. Hum Mol Genet 24:5313–5325. https://doi.org/10.1093/hmg/ddv250
14. Romaniello R, Arrigoni F, Panzeri E et al (2017) Erratum to: Tubulin-related cerebellar dysplasia: definition of a distinct pattern of cerebellar malformation. Eur Radiol 27:5093. https://doi.org/10.1007/s00330-017-4986-6
15. Romaniello R, Tonelli A, Arrigoni F et al (2012) A novel mutation in the β-tubulin gene TUBB2B associated with complex malformation of cortical development and deficits in axonal guidance. Dev Med Child Neurol 54:765–769. https://doi.org/10.1111/j.1469-8749.2012.04316.x
16. Kamiya K, Tanaka F, Ikeno M et al (2014) DTI tractography of lissencephaly caused by TUBA1A mutation. Neurol Sci 35:801–803. https://doi.org/10.1007/s10072-014-1662-3
17. Poretti A, Meoded A, Rossi A et al (2013) Diffusion tensor imaging and fiber tractography in brain malformations. Pediatr Radiol 43:28–54. https://doi.org/10.1007/s00247-012-2428-9
18. Poretti A, Boltshauser E, Loenneker T et al (2007) Diffusion tensor imaging in Joubert syndrome. AJNR Am J Neuroradiol 28:1929–1933. https://doi.org/10.3174/ajnr.A0703
19. Arrigoni F, Romaniello R, Peruzzo D et al (2017) Anterior mesencephalic cap dysplasia: novel brain stem malformative features associated with Joubert syndrome. AJNR Am J Neuroradiol 38:2385–2390. https://doi.org/10.3174/ajnr.A5360
20. Sicotte NL, Salamon G, Shattuck DW et al (2006) Diffusion tensor MRI shows abnormal brainstem crossing fibers associated with ROBO3 mutations. Neurology 67:519–521. https://doi.org/10.1212/01.wnl.0000227960.38262.0c
21. Severino M, Tortora D, Pistorio A et al (2016) Expanding the spectrum of congenital anomalies of the diencephalic-mesencephalic junction. Neuroradiology 58:33–44. https://doi.org/10.1007/s00234-015-1601-x
22. Poretti A, Boltshauser E, Huisman TAGM (2016) Cerebellar and brainstem malformations. Neuroimaging Clin N Am 26:341–357. https://doi.org/10.1016/j.nic.2016.03.005
23. Peruzzo D, Arrigoni F, Triulzi F et al (2014) Detection of corpus callosum malformations in pediatric population using the

discriminative direction in multiple kernel learning. Med Image Comput Comput Assist Interv 17:300–307
24. Kweldam CF, Gwynn H, Vashist A et al (2014) Undecussated superior cerebellar peduncles and absence of the dorsal transverse pontine fibers: a new axonal guidance disorder? Cerebellum 13:536–540. https://doi.org/10.1007/s12311-014-0562-7
25. Avadhani A, Ilayaraja V, Shetty AP, Rajasekaran S (2010) Diffusion tensor imaging in horizontal gaze palsy with progressive scoliosis. Magn Reson Imaging 28:212–216. https://doi.org/10.1016/j.mri.2009.10.004
26. Calloni SF, Cohen JS, Meoded A et al (2017) Pediatric neurology compound heterozygous variants in ROBO1 cause a neurodevelopmental disorder with absence of transverse pontine fibers and thinning of the anterior commissure and corpus callosum. Pediatr Neurol 70:70–74. https://doi.org/10.1016/j.pediatrneurol.2017.01.018
27. Rollins NK, Booth TN, Chahrour MH (2017) Variability of pontocerebellar fibers by diffusion tensor imaging in diverse brain malformations. J Child Neurol 32:271–285. https://doi.org/10.1177/0883073816680734
28. Pierpaoli C, Walker L, Irfanoglu MO et al (2010) Tortoise: an integrated software package for processing of diffusion MRI data. In: Proceedings of the annual meeting of the International Society for Magnetic Resonance in Medicine (ISMRM 2010), 1–7 May 2010. Stockholm, Sweden, p. 1597
29. Basser PJ, Pierpaoli C (2011) Microstructural and physiological features of tissues elucidated by quantitative-diffusion-tensor MRI. 1996. J Magn Reson 213:560–570. https://doi.org/10.1016/j.jmr.2011.09.022
30. Pajevic S, Pierpaoli C (1999) Color schemes to represent the orientation of anisotropic tissues from diffusion tensor data: application to white matter fiber tract mapping in the human brain. Magn Reson Med 42:526–540
31. Rohde GK, Barnett AS, Basser PJ et al (2004) Comprehensive approach for correction of motion and distortion in diffusion-weighted MRI. Magn Reson Med 51:103–114. https://doi.org/10.1002/mrm.10677
32. Chang LC, Jones DK, Pierpaoli C (2005) RESTORE: robust estimation of tensors by outlier rejection. Magn Reson Med 53:1088–1095. https://doi.org/10.1002/mrm.20426
33. Wang R, Benner T, Sorensen AG (2007) Diffusion toolkit: a software package for diffusion imaging data processing and tractography. In: Proceedings of the 15th Meeting of the International Society for Magnetic Resonance in Medicine, Berkeley, p. 3720
34. Wang K, Li M, Hakonarson H (2010) ANNOVAR: functional annotation of genetic variants from high-throughput sequencing data. Nucleic Acids Res 38:e164. https://doi.org/10.1093/nar/gkq603
35. Flores-Sarnat L (2002) Hemimegalencephaly: part 1. Genetic, clinical, and imaging aspects. J Child Neurol 17:373–384; discussion 384. https://doi.org/10.1177/088307380201700512
36. Barkovich AJ, Dobyns WB, Guerrini R (2015) Malformations of cortical development and epilepsy. Cold Spring Harb Perspect Med 5:a022392. https://doi.org/10.1101/cshperspect.a022392
37. Chan WM, Traboulsi EI, Arthur B et al (2006) Horizontal gaze palsy with progressive scoliosis can result from compound heterozygous mutations in ROBO3. J Med Genet 43:e11. https://doi.org/10.1136/jmg.2005.035436
38. Jissendi-Tchofo P, Severino M, Nguema-Edzang B et al (2015) Update on neuroimaging phenotypes of mid-hindbrain malformations. Neuroradiology 57:113–138. https://doi.org/10.1007/s00234-014-1431-2
39. Barkovich AJ (2012) Developmental disorders of the midbrain and hindbrain. Front Neuroanat 6:7. https://doi.org/10.3389/fnana.2012.00007
40. Jen JC, Chan W-M, Bosley TM et al (2004) Mutations in a human ROBO gene disrupt hindbrain axon pathway crossing and morphogenesis. Science 304:1509–1513. https://doi.org/10.1126/science.1096437
41. Engle EC (2010) Human genetic disorders of axon guidance. Cold Spring Harb Perspect Biol 2:a001784. https://doi.org/10.1101/cshperspect.a001784
42. Friede RL, Boltshauser E (1978) Uncommon syndromes of cerebellar vermis aplasia. I: Joubert syndrome. Dev Med Child Neurol 20:758–763
43. Ferland RJ, Eyaid W, Collura RV et al (2004) Abnormal cerebellar development and axonal decussation due to mutations in AHI1 in Joubert syndrome. Nat Genet 36:1008–1013. https://doi.org/10.1038/ng1419
44. Miyata H, Miyata M, Ohama E (2014) Pyramidal tract abnormalities in the human fetus and infant with trisomy 18 syndrome. Neuropathology 34:219–226. https://doi.org/10.1111/neup.12081
45. ten Donkelaar HJ, Lammens M, Wesseling P et al (2004) Development and malformations of the human pyramidal tract. J Neurol 251:1429–1442. https://doi.org/10.1007/s00415-004-0653-3
46. Walker L, Chang L-C, Nayak A et al (2016) The diffusion tensor imaging (DTI) component of the NIH MRI study of normal brain development (PedsDTI). Neuroimage 124:1125–1130. https://doi.org/10.1016/j.neuroimage.2015.05.083
47. Nayak A, Sadeghi N, Irfanoglu MO et al (2017) Diffusion-tensor based morphometry of normal human development from infancy to adulthood. In: Proceedings of the 25th Annual Meeting of the International Society for Magnetic Resonance in Medicine (ISMRM), 22-27 April 2017, Honolulu, p. 3371